Check for updates

Advanced Sustainable Systems

ADVANCED SUSTAINABLE SYSTEMS
www.advsustainsys.com

RESEARCH ARTICLE OPEN ACCESS

Integrated Valorization of Waste Biomass via Low-Temperature Pyrolysis and Biochar Application as Heterogeneous Catalyst for SAF Production

Nicola Schiaroli[1] | Lorenzo Scaglione[1] | Marzia Ortelli[1] | Sonia Blasioli[1,2] | Ilaria Braschi[2] | Sandro Recchia[1] | Massimo Mella[1] | Carlo Lucarelli[1]

[1]Dipartimento di Scienza e Alta Tecnologia, Università degli Studi dell'Insubria, Como, Italy | [2]Dipartimento di Scienze e Tecnologie Agro-Alimentari, Alma Mater Studiorum – Università di Bologna, Bologna, Italy

Correspondence: Nicola Schiaroli (nicola.schiaroli@uninsubria.it)

Received: 22 January 2026 | **Revised:** 24 April 2026 | **Accepted:** 28 April 2026

Keywords: aldol condensation | biochar | biorefinery | heterogeneous catalysis | pyrolysis | sustainable aviation fuel | waste management

ABSTRACT

Common waste biomasses such as fruit and vegetable peels and spent coffee grounds are valorized via low-temperature pyrolysis (400°C) to produce valuable biochar and bio-oil for diverse downstream applications. Detailed and comprehensive characterization of the resulting biochar, including carbonization degree, morphology, surface acidity/basicity, and energy content, enables the assessment of their suitability for technological and environmental uses, based on the specific properties developed during thermal conversion. The bio-oils exhibit feedstock-dependent chemical profiles enriched in platform chemicals (e.g., HMF, furfural, cyclic ketones), lipid-derived compounds, and aromatics, supporting their targeted utilization in energy, materials, and chemical synthesis. Upon sulfonation, selected biochars display promising properties as acidic heterogeneous catalysts (1.65–1.75 mmol H^+ g^{-1}), showing high activity in industrially relevant reactions such as esterification and condensation. Their application in the cross-aldol condensation between bio-based cyclopentanone and cyclohexanone, targeting sustainable aviation fuel (SAF) precursors (C_{10}-C_{18} cyclic compounds), is explored in detail. Among all samples, sulfonated biochar derived from coffee grounds and orange peel achieves superior catalytic performance, matching or surpassing commercial Amberlyst-15 under mild conditions (120°C, 4 h, atmospheric pressure). Catalyst stability and recyclability tests confirm performance retention after regeneration, with surface deactivation by heavy compounds deposition being fully reversible.

1 | Introduction

Rising environmental concerns, population growth, and the increasing demand for energy, chemicals, and materials have driven research into low-impact technologies using renewable raw materials. Technologies like pyrolysis, gasification, biogas upgrading [1, 2], CO_2 valorization [3, 4] can convert waste into high-value products such as fuel [5], chemicals [6, 7], H_2, heat, and electricity [8]. Pyrolysis involves the thermal degradation of organic matter in the absence of oxygen to produce a condensable fraction (bio-oil), a gaseous mixture (mainly composed of CO, H_2, CH_4, and light hydrocarbons), and a solid residue called biochar. The valorization of bio-oil derived from food and green waste has gained considerable attention due to its potential as a renewable energy source and chemical feedstock for industrial processes, including the production of valuable chemicals (such as intermediates, solvents, plastics) and fuels [9]. On the other hand, biochar (BC), a solid carbon-rich material, finds applications as a solid fuel [10], soil amendment [11], and pollutant adsorption [12]. Another interesting application of BC lies in its potential

This is an open access article under the terms of the Creative Commons Attribution License, which permits use, distribution and reproduction in any medium, provided the original work is properly cited.
© 2026 The Author(s). *Advanced Sustainable Systems* published by Wiley-VCH GmbH

use as a support material or catalyst for several reactions of industrial relevance, such as biodiesel synthesis [13], hydrocracking [14], desulfurization [15], and syngas production [16]. To be employed for these purposes, BC typically undergoes a previous activation process aimed at increasing its surface area/porosity, functionalizing it with acidic or basic groups, or modifying it to facilitate the incorporation of metallic or oxide nanoparticles [17–19]. In this context, sulfonation is a cost-effective process that can effectively activate BC, increasing its surface acidity by the addition of sulfonic acid (—SO_3H) and oxygenated (—COOH) groups [20] through its treatment with different agents such as para-toluene sulfonic acid (p-TSA), chlorosulfonic acid (HSO_3Cl), tosylic acid (TsOH), or H_2SO_4 [21]. Sulfonated biochar (SBC) was successfully utilized as a heterogeneous catalyst for the synthesis of biodiesel from oleic acid with a maximal yield of 98% at 75°C [22]. Kumari et al. [23]. applied SBC derived from pine needles in the conversion of fructose to levulinic acid (yield of 33% at 180°C after 6 h) and further esterification to ethyl levulinate (yield of 97% at 50°C after 17 h). In this case, chlorosulfonic acid was used for BC treatment, but no data regarding catalyst deactivation were reported. The hydrolysis of maltose to glucose was investigated by Xiong et al. [24]. obtaining high yields, especially at low temperatures (140°C–160°C) and a selectivity toward HMF of 60% when SBC was applied also as the catalyst for fructose dehydration. SBC obtained via hydrothermal carbonization of orange peel was found to be highly active in the reaction between 2-methylfuran and furfural for the synthesis of a C_{15} biofuel precursor [25]. In optimized conditions, a product yield of 83% was attained at 50°C after 5 h of reaction, but a significant deactivation was observed after four reaction cycles, when C_{15} yield decreased to a value of 48%. This deactivation was attributed to both the formation of undesired heavy compounds that blocked the catalyst active sites and a partial leaching of the sulfonic groups, whose surface concentration decreased from 2.148 mmol g^{-1} to a value of 1.340 mmol g^{-1} during consecutive reactions. Starting from the pyrolysis of oil-tea shell and using benzenesulfonic acids and 4-tert-butylaniline for BC activation, Zhong et al. [26]. were able to obtain superacid BC with great hydrophobicity that enhanced its activity and stability in the alkylation reaction of 4-ethylphenol-phenylmethanol and 2-methylfuran-cyclic ketones for the synthesis of renewable and high-density fuel precursors (C_{15}-C_{22}) with high efficiency even after 5 reaction cycles. In this framework, the present study demonstrates a comprehensive biorefinery approach by valorizing common food waste (fruit-vegetables peels and coffee grounds) through low-temperature pyrolysis (400°C). The chemical profiling of the resulting bio-oils reveals feedstock-dependent chemical compositions, ranging from aromatic-rich mixtures to platforms high in furfurals and HMF, highlighting their potential as chemical intermediates. Simultaneously, the solid biochars were thoroughly investigated through SEM, FT-ATR, TG, and CHN analyses to correlate their carbonization degree and surface chemistry with their functional properties. These materials were functionalized and tested as acid catalysts for reactions of industrial relevance, such as the production of sustainable aviation fuel (SAF). In this context, the cross-aldol condensation between bio-based cyclopentanone and cyclohexanone was investigated using, for the first time, biochar-based catalysts with the aim of demonstrating an integrated approach to biomass waste upgrading within a biorefinery framework.

2 | Results and Discussion

2.1 | Biochar and Bio-Oil Characterization

The various waste biomasses, namely spent coffee grounds (CG), orange peel (OP), pineapple peel (PP), banana peel (BP), and green waste (GW, scraps of broad-leaved vegetables such as chard and lettuce) were carbonized at low-temperature pyrolysis conditions of 300°C and 400°C. The influence of temperature is depicted in Figure S1. As a general trend, an increase in process temperature corresponds to a lowering of BC yield. Between the different substrates, GW reached the highest BC yields both at 300°C (80%) and 400°C (53%), while CG showed a marked tendency to degradation, hitting a BC yield of 30% at 400°C. A detailed representation of bio-oil and BC yields at 400°C is shown in Figure 1a. Between the different substrates, CG degradation produced the highest yield in bio-oil (31%), followed by OP and PP (26% for both). Comparing the results obtained with those of biomass and BC ultimate analyses (CHN, Figure 1b,c, respectively), it can be observed that waste thermal degradation at 400°C led to a significant increase of C concentration (see Table S1 for further data about pristine biomass and biochar samples obtained at 300°C).

In detail, it is possible to calculate a Carbon densification percentage (expressed as the percentage increase in carbon content following pyrolysis) that qualitatively expresses the tendency of the substrate to thermal degradation/deoxygenation through decarboxylation, dehydration, depolymerization, demethanation reactions [27], which occurs more effectively in the following order: GW (+32%) < BP < CG < PP < OP (+61%). It should be noted, however, that CG showed the highest C concentration after pyrolysis at 400°C (74%) and the lowest volatiles content (42.8% as reported in Table 1), confirming its higher carbonization degree. The changes registered in terms of C, H, and O concentrations after thermal degradation resulted in a significant decrease in H/C and O/C atomic ratios of the various BCs. The Van Krevelen diagram displayed in Figure 1d shows the comparison between the H/C and O/C atomic ratios of the BCs obtained at 400°C and those that typically characterize common carbonaceous materials such as anthracite, bituminous coal, lignite, and peat. In this context, lower ratios indicate a higher aromaticity of the substrates, where the decreased of O/C ratio expresses the elimination of hydrophilic functional groups [28] while the lowering of the H/C ratio suggests a higher structural stability [29]. The possible application of BC as a solid fuel is typically analyzed through the calculation of its higher heating value (HHV), which increases following the order GW < BP < PP < OP < CG in accordance with the thermal degradation behavior observed during pyrolysis. Remarkably, the HHV of CG (28.5 MJ Kg^{-1}, BC obtained at 400°C) was found to be comparable with that of bituminous coal, while those of OP, PP, and GW fall within the values that typically characterize lignite materials [30].

The SEM images of the various BCs obtained at 400°C (Figure S2) show different surface morphologies depending on the starting biomass, with varying amounts of visible macropores, especially in the case of OP and CG. Remarkably, in PP and BP samples, a significant presence of particles was observed, distributed across the entire surface of the substrate (Figure S3). Their

23667486, 2026, 5, Downloaded from https://advanced.onlinelibrary.wiley.com/doi/10.1002/adsu.70489 by Ilaria braschi - Area Sistemi Dipart & Doc , Wiley Online Library on [11/05/2026]. See the Terms and Conditions (https://onlinelibrary.wiley.com/terms-and-conditions) on Wiley Online Library for rules of use; OA articles are governed by the applicable Creative Commons License

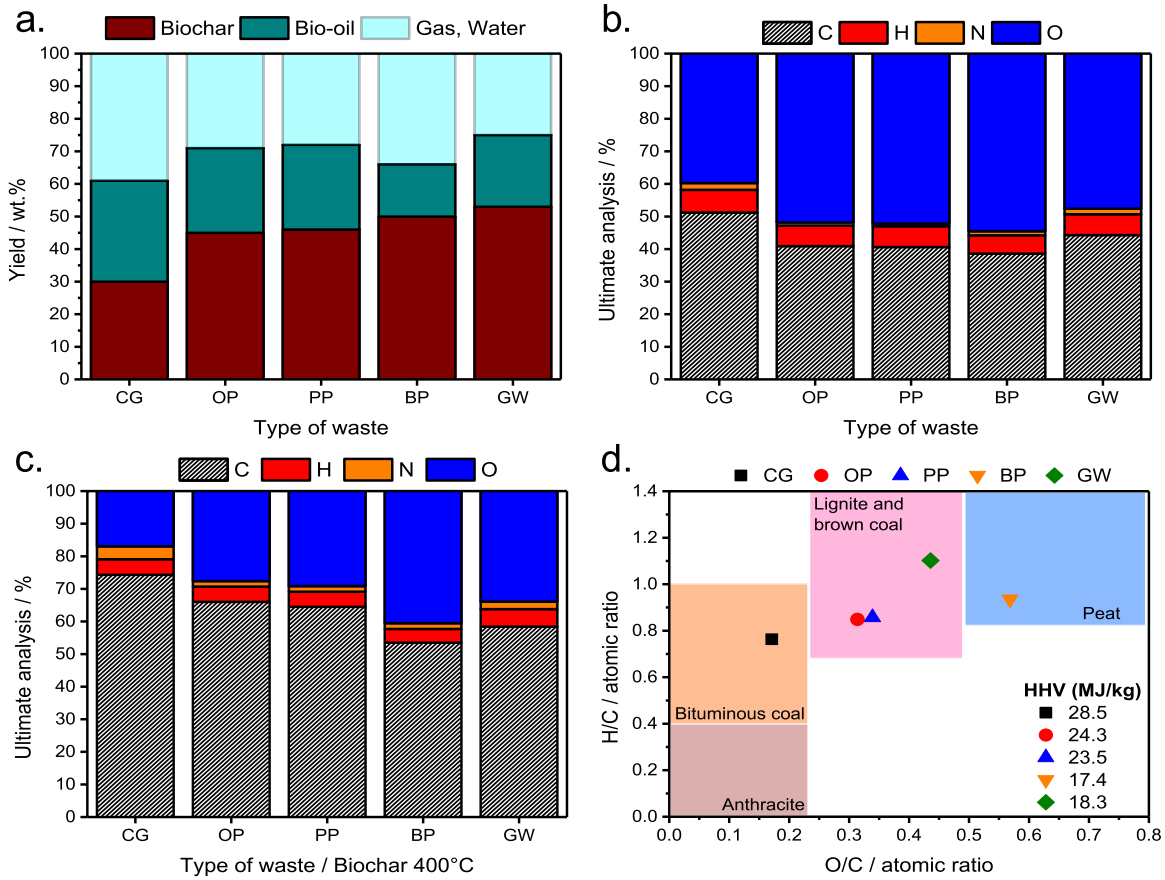

FIGURE 1 | (a) Yields of BC and bio-oil (organic phase only) for biomass waste after pyrolysis at 400°C for 1 h; CHN analyses of (b) biomass and (c) BC obtained at 400°C; (d) Van Krevelen diagram of BC obtained at 400°C with corresponding HHV values. CG: coffee grounds, OP: orange peel, PP: pineapple peel, BP: banana peel, GW: green waste.

TABLE 1 | Proximate analyses of pristine biomass waste (on dry basis) and volatiles content of samples after pyrolysis at 400°C for 1 h.

Type of Waste	Volatiles [%]	Fixed Carbon [%]	Ash [%]	BC-400 Volatiles [%][a]
CG	83.31	14.15	2.54	42.8 (−49%)
OP	80.70	17.46	1.84	67.4 (−16%)
PP	73.73	26.16	0.11	44.1 (−40%)
BP	76.01	15.53	8.46	54.8 (−28%)
GW	80.82	10.45	8.73	63.0 (−22%)

[a]The values in parentheses indicate the percentage loss relative to the sample prior to pyrolysis.

inorganic nature was confirmed through EDX analyses, which identified the presence of K-salts, with an atomic concentration exceeding 6% for the BP sample, in accordance with the high ash content determined through proximate analysis of pristine biomass (8.46 wt.%, Table 1). This explains its pronounced basic behavior when dispersed into water (Table 2), suggesting its possible application as an adsorption material for environmental applications [31, 32] such as the recovery of nutrients or the decontamination of wastewaters [33, 34].

Among all the samples observed after pyrolysis, CG shows the most visible surface roughness and a microstructure characterized by a high density of cavities uniformly distributed throughout the sample (Figure S4). This feature is likely attributable both to the higher volatile content lost during pyrolysis (−49% starting from 83.30% in pristine biomass, Table 1) and to the roasting treatment, which is typically part of the coffee production process [35]. Moreover, different from the other samples, CG is characterized by a significant acidic character (0.490 mmol H^+ g^{-1}), probably associated with the contribution of -COOH groups at its surface and to a scarce presence of basic salts, as confirmed from the EDX analysis (overall atomic concentration ~ 0.6%, Figure S4).

The FT-ATR spectra of biomass waste, reported in Figure 2a, show the presence of main functional groups characteristic of lignocellulosic materials [36]. The broad band centered at ~ 3300 cm^{-1} can be attributed to the stretching of O—H (and N—H) groups present in carbohydrates, fatty acids, and proteins [37]. The two peaks at

23667486, 2026, 5, Downloaded from https://advanced.onlinelibrary.wiley.com/doi/10.1002/adsu.70489 by Ilaria Braschi - Area Sistemi Dipart & Doc , Wiley Online Library on [11/05/2026]. See the Terms and Conditions (https://onlinelibrary.wiley.com/terms-and-conditions) on Wiley Online Library for rules of use; OA articles are governed by the applicable Creative Commons License

TABLE 2 | Measured contact angles between different biochar and water (sessile drop method) and pH of biochar with corresponding basicity/acidity values.

Type of Waste (Biochar)	BC contact angle [°]		BC-400 pH/[mmol OH^- g^{-1}]
	300°C	400°C	
CG	101.7	107.8	4.0 / [0.490 H^+]
OP	115.0	116.3	7.2 / [0.220]
PP	93.7	99.4	7.1 / [0.125]
BP	93.3	95.3	10.7 / [1.459]
GW	84.1	92.1	9.5 / [0.687]

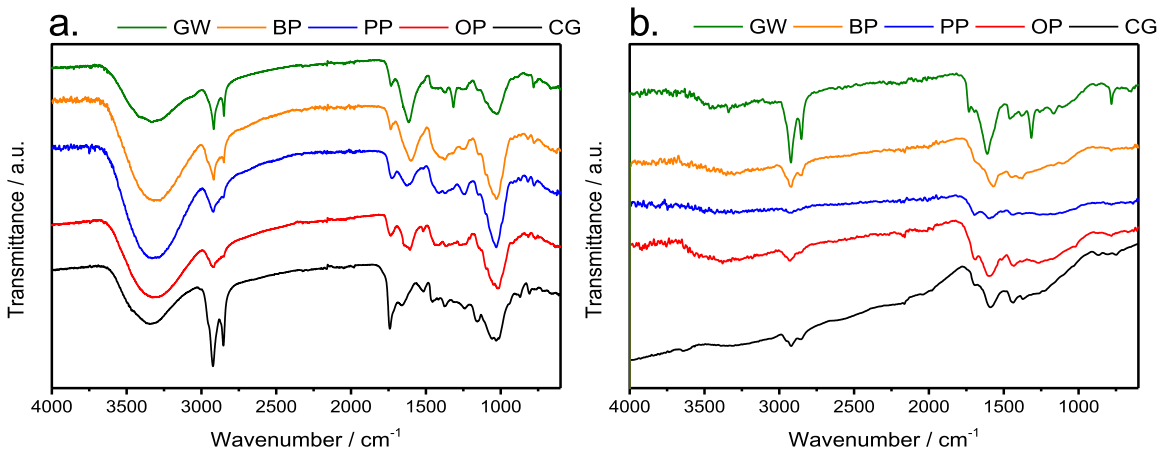

FIGURE 2 | FT-ATR spectra of (a) waste biomass and (b) BCs obtained after pyrolysis at 400°C. CG: coffee grounds, OP: orange peel, PP: pineapple peel, BP: banana peel, GW: green waste.

2920 and 2850 cm^{-1}, particularly narrow in the case of CG, BP, and GW biomasses, are associated with symmetrical stretching of —CH_3 and asymmetrical stretching of —CH_2-, typical of lipidic structures. The common peak at 1730–1740 cm^{-1} corresponds to carbonyl bond (C═O) vibrations, typical of ester functional groups of hemicelluloses. The signals comprise in the range 1600–1660 $cm^{-1}$are attributable to both C═C bond stretching and N-H primary amine bending of proteins [38], while the peaks at 1600–1450 cm^{-1} are associated with C—C skeletal vibrations of aromatics that, together with the signals at 1310–1390 cm^{-1}(O—H bending of phenol), are derived from different percentages of lignin fraction between samples. The presence of C—O—C bonds of polysaccharides compounds is revealed by the various peaks recorded in the region 1000–1150 cm^{-1}, while the signals between 770–900 cm^{-1} are attributable to C—H bending typical of lignin and cellulose [39]. After pyrolysis at 400°C, the FT-ATR spectra of the obtained BCs (Figure 2b) are mainly characterized by the presence of peaks associated with C—H vibrations typical of carbonaceous materials, and broad and weak signals attributable to the presence of O—H, C—O—C, and C═O vibrational modes, in accordance to the results obtained from CHN analyses of samples (Figure 1c). It is noteworthy that among the different biomasses after pyrolysis, the GW spectrum shows more defined peaks that, resembling those of pristine biomass, confirm a lower degradation of the starting material, in agreement both with both the high BC yield obtained after thermal decomposition (Figure 1a) and the elevated volatiles content that characterized GW biochar obtained after low-temperature pyrolysis (63.0 wt.% at 400°C).

The loss observed in terms of oxygenated functional groups during degradation (as also observed from CHN analyses) leads to an increasing hydrophobic behavior with pyrolysis temperature, as evidenced by the measured contact angles between water and BCs surface assessed through the sessile drop method (Table 2). In detail, the determined contact angle values increase with thermal degradation temperature, evidencing a marked hydrophobic surface for both OP and CG samples at 400°C (116.3° and 107.8°, respectively) in accordance with their low H/C and O/C ratio values. In this context, considering the various samples analyzed, the BCs obtained from PP, GW, and BP, exhibiting lower hydrophobicity (contact angles of 84°–100°) and a neutral to alkaline behavior in water, can be regarded as promising candidates for potential use as amendments in acidic soils [40], given that increasing soil pH is associated with higher crop yields [41], while, due to the marked hydrophobicity and/or acidity, OP and CG do not meet these criteria [42].

The structural and compositional changes that biomasses undergo during pyrolysis are reflected in the composition and nature of the bio-oil produced from the condensation of the volatiles released during the thermal degradation process. The results of the various samples in terms of qualitative compositional distributions, expressed as percentage areas, are shown

23667486, 2026, 5, Downloaded from https://advanced.onlinelibrary.wiley.com/doi/10.1002/adsu.70489 by Ilaria Braschi - Area Sistemi Dipart & Doc , Wiley Online Library on [11/05/2026]. See the Terms and Conditions (https://onlinelibrary.wiley.com/terms-and-conditions) on Wiley Online Library for rules of use; OA articles are governed by the applicable Creative Commons License

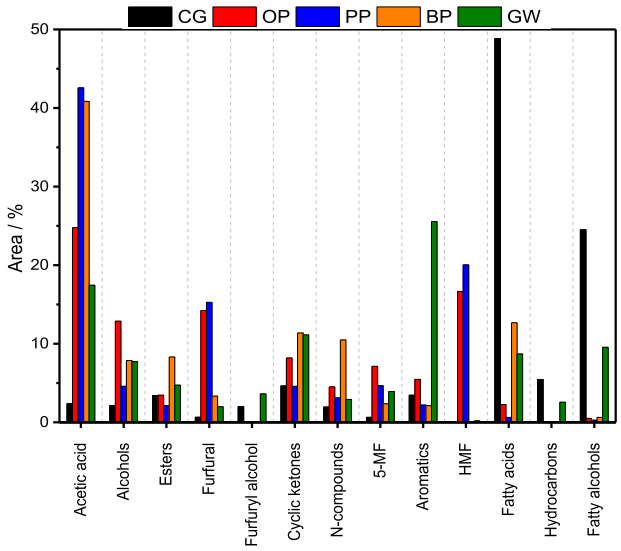

FIGURE 3 | Bio-oils qualitative composition as obtained from GC-MS analyses. The liquids were collected during pyrolysis experiments conducted at 400°C. CG: coffee grounds, OP: orange peel, PP: pineapple peel, BP: banana peel, GW: green waste.

in Figure 3. As can be observed, the bio-oils were composed of a wide range of oxygenated compounds (see Figure S5 for detailed information on the main molecules identified), and the presence/relative abundance of specific classes of compounds varies significantly depending on the type of feedstock. In detail, OP and PP yield bio-oils particularly rich in industrially relevant compounds such as acetic acid, hydroxymethylfurfural (HMF), and furfural. While acetic acid (especially abundant also in BP-oil) is generally formed from decomposition of simple sugars [43], the two latter (together with esters and alcohols) are generally associated with the hydrolysis/dehydration of polysaccharides such as cellulose and hemicellulose and are considered important platform molecules to produce renewable plastics, fuels, solvents, and high added value chemicals [44, 45]. Cyclic ketones (evolved from the majority of substrates, expect from CG) can be upgraded to high energy-density compounds through various bottom-up methods to produce promising sustainable aviation fuels (SAF) [5, 46] while a significant presence of aromatic compounds (as in the case of GW-oil), besides being associated with a higher lignin content in the starting biomass, makes the mixture suitable for use in the synthesis of green fuels, solvents and fine chemicals [47–49]. Notably, CG-oil is especially rich in fatty acids/alcohols and hydrocarbons, likely originated from the decomposition of lipid structures, and shows only small percentages of the other classes of compounds. This can likely be attributed to the water extraction process occurring during coffee brewing, which makes this bio-oil particularly suitable to produce valuable products such as biodiesel, surfactants, lubricants, and intermediates [50, 51].

2.2 | Biochar Activation Through Sulfonation

The BCs produced at 400°C were subjected to chemical activation through sulfonation treatment. All FT-ATR spectra recorded for the various samples (Figure 4a) confirmed the successful surface functionalization, as indicated by the appearance of new bands in the 900–1300 cm^{-1} region. These signals can be attributed both to C—O—C bonds and sulfonic groups (—SO_3H) stretching [52].

Additionally, the signal observed around 635 cm^{-1} is consistent with the stretching vibration of the C—S bond and, along with the reappearance of detectable —OH functional groups, further confirms the presence of new chemical functionalities on the material surface [53]. It is noteworthy that during the activation process, part of the substrate is degraded by the strong acidic/oxidizing environment as revealed by the general trend toward a reduction in C concentration detected by CHN analyses (Figure S6) and confirmed also by the disappearance of the peaks associated with —CH_3 stretching (around 2900 cm^{-1}) in favor of the intensification of the signal of C═O functional groups (1700 cm^{-1}) after sulfonation. In the case of GW, this tendency is less pronounced and indicates a higher degree of chemical stability. Figure 4b shows the surface density of acid sites measured after sulfonation for the different samples. Although a clear correlation between the measured values and the properties of the various BCs cannot be easily established, the observed trend suggests that activation tends to be more effective in samples that experienced greater carbon densification during pyrolysis. Consequently, OP and CG show the highest concentration values, 1.73 and 1.66 mmol H^+ g^{-1}, respectively, while GW exhibits a poor total acidity of 1.09 mmol H^+ g^{-1}. Although the samples were characterized by a limited surface area (SS_{BET} < 2 m^2 g^{-1}), the SEM images revealed a general increase in the surface roughness, with some smooth areas still observable. As confirmed by EDX analyses, the acid treatment leads to the dissolution of inorganic salts previously present in the BCs (Figure S7), thus excluding their possible role in BCs catalytic properties.

The images of the two samples with the highest surface acidity are shown in Figure 5. A different morphology was observed: the microstructure characterized by open cavities in the CG sample appears to be enhanced by the sulfonation process, while the OP sample exhibits a larger number of flat areas, possibly indicating a lower degree of biochar degradation during activation. Interestingly, CG also exhibits the formation of small, discrete cavities distributed across its surface, with diameters below 1 μm.

2.3 | Biochar as Heterogeneous Catalyst

Given their promising characteristics, the activated OP and CG were selected as candidates for catalytic evaluation and subsequently tested in two reactions of industrial interest (Figure 6a). In both cases, the results were compared with those obtained using Amberlyst-15, a commercial styrene-divinylbenzene sulfonated resin with a total acidity of 4.70 mmol H^+ g^{-1} [54]. The esterification reaction between propionic acid (PA) and n-butanol (BuOH, both obtainable from green sources [55]) to give butyl propionate, a product with wide application as fruit aroma, solvent for resin, paints and coatings industry [56], was carried out at 80°C using a constant amount of acid sites in the reaction system (0.15 mmol H^+ $g_{reagents}^{-1}$). The results reported in Figure 6b show that, although characterized by significantly lower acidity, sulfonated BCs exhibited a catalytic activity comparable (or

23667486, 2026, 5, Downloaded from https://advanced.onlinelibrary.wiley.com/doi/10.1002/adsu.70489 by Ilaria braschi - Area Sistemi Dipart & Doc , Wiley Online Library on [11/05/2026]. See the Terms and Conditions (https://onlinelibrary.wiley.com/terms-and-conditions) on Wiley Online Library for rules of use; OA articles are governed by the applicable Creative Commons License

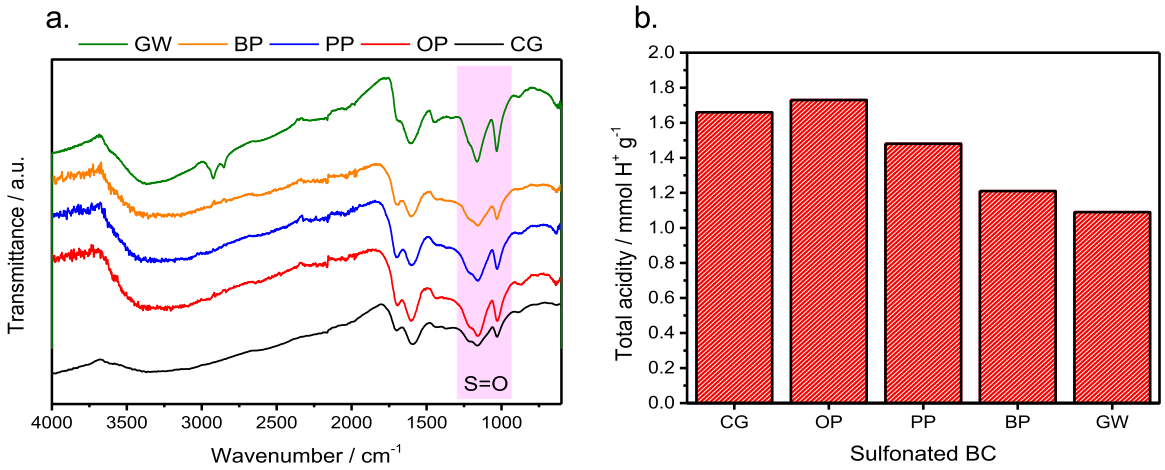

FIGURE 4 | (a) FT-ATR spectra of the sulfonated BCs and (b) total acidity of the various samples after sulfonation expressed as mmol H^+/g. CG: coffee grounds, OP: orange peel, PP: pineapple peel, BP: banana peel, GW: green waste.

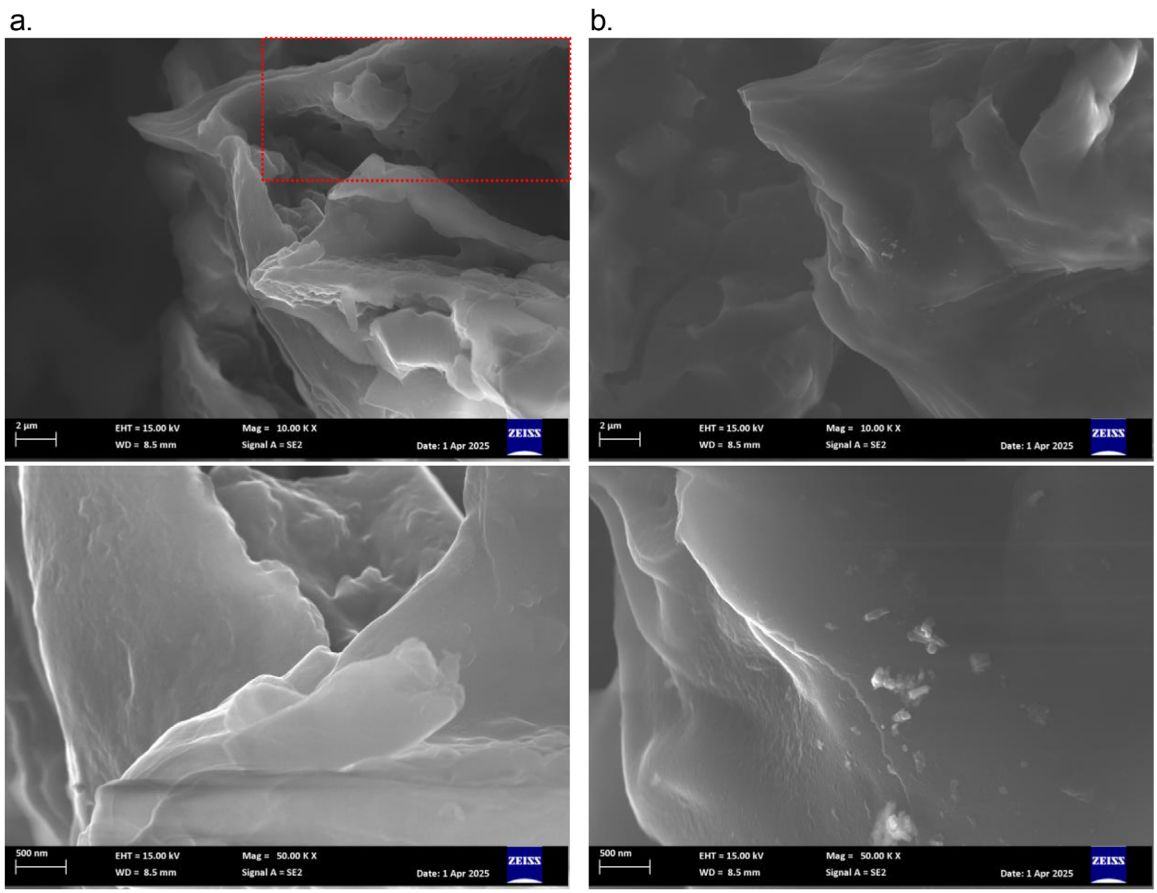

FIGURE 5 | SEM images of samples after sulfonation: (a) CG (the red square evidences a zone rich in discrete cavities) and (b) OP. CG: coffee grounds, OP: orange peel.

slightly superior) than that of Amberlyst-15, demonstrating that, in this case, the acidic sites display nearly identical intrinsic activity. Notably, the difference of surface acidity besides CG and OP is not reflected in the reaction output, when used in a second reaction cycle without any regeneration treatment, both catalysts showed no significant loss of activity.

The second process regards the cross-aldol condensation of cyclopentanone and cyclohexanone (CPO and CHE, both obtainable from biomass) to give C10-C18 cyclic ketones, which are considered as promising precursors of high-energy-density sustainable aviation fuel (SAF) [46]. Also in this case, the preliminary catalytic tests were conducted using a constant amount of acid

23667486, 2026, 5, Downloaded from https://advanced.onlinelibrary.wiley.com/doi/10.1002/adsu.70489 by Ilaria Braschi - Area Sistemi Dipart & Doc , Wiley Online Library on [11/05/2026]. See the Terms and Conditions (https://onlinelibrary.wiley.com/terms-and-conditions) on Wiley Online Library for rules of use; OA articles are governed by the applicable Creative Commons License

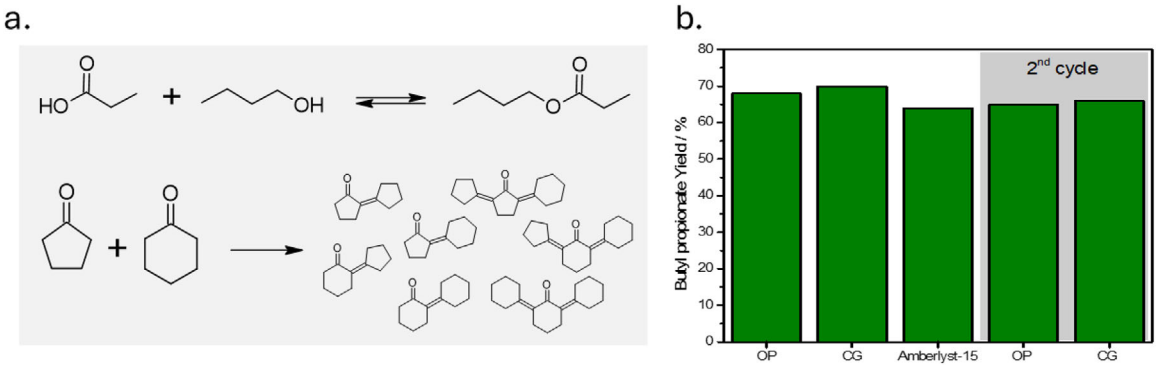

FIGURE 6 | (a) Esterification reaction between propionic acid and n-butanol, and cross-aldol condensation between cyclopentanone and cyclohexanone. (b) Catalytic results in terms of butyl propionate yield for OP, CG, and Amberlyst-15. The results of BC catalysts recyclability are reported on the right. Reaction conditions: PA = 22 mmol, BuOH = 22 mmol, T = 80°C, time = 4 h, catalyst amount = 0.15 mmol H^+ $g_{reagents}^{-1}$. CG: coffee grounds, OP: orange peel.

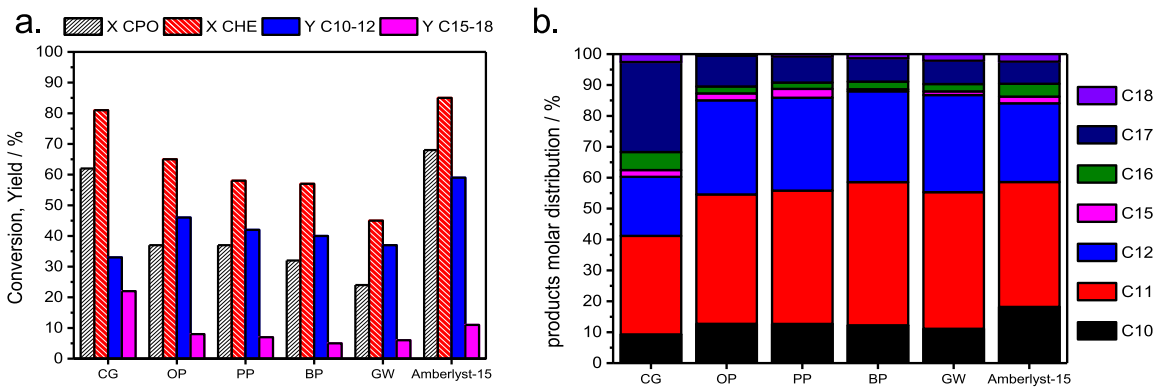

FIGURE 7 | Catalytic activity in cross-aldol condensation of sulfonated BCs and Amberlyst-15: (a) catalyst performance in terms of CPO, CHE conversions (X CPO, CHE) and product yields (Y C10-12 and Y C15-18); (b) molar fraction of the different compounds in the product mixture. Reaction conditions: CPO = 22 mmol, CHE = 22 mmol, T = 120°C, time = 4 h, catalyst amount = 0.15 mmol H^+ $g_{(CPO+CHE)}^{-1}$. Total acidity for BCs is reported in Figure 5b, Amberlyst-15 acidity = 4.70 mmol H^+ g^{-1}. CG: coffee grounds, OP: orange peel, PP: pineapple peel, BP: banana peel, GW: green waste, CPO: cyclopentanone, CHE: cyclohexanone.

sites in the system (0.15 mmol H^+ $g_{(CPO+CHE)}^{-1}$) in solvent-free conditions but operating at 120°C for 4 h. The results obtained for the various sulfonated BCs are reported in Figure 7a, expressed in terms of CPO and CHE conversions (X_{CPO}, X_{CHE}) and C10-12 and C15-18 product yields (Y_{C10-12}, Y_{C15-18}). Unlike esterification, the reaction output of this process strongly depends on the intrinsic activity of the various catalysts, which therefore exhibit significantly different results, partly reflecting their trend in terms of total surface acidity. The activity of the GW catalyst is low, with CPO and CHE conversions of 24% and 45%, respectively, while BP and PP showed similar catalytic performance, hitting C10-12 yields around 40%. It is noteworthy that, regardless of catalyst nature, CHE is more reactive in the considered system, consistently showing conversion values significantly higher than those of CPO. This is particularly true for the OP sample that exhibited a X_{CHE} of 66%, approximately 43% greater than X_{CPO}, and a Y_{C10-12} of 46%, which is the highest among the various BCs tested.

Although Amberlyst-15 shows the highest conversion (and superior Y_{C10-12} of 59%), the CG catalyst exhibits comparable activity in terms of CPO and CHE reactivity. Specifically, the intrinsic activity, calculated as the ratio of mmol of converted reagents to the mmol of acid sites over a 4 h reaction period [54], was 13.08 h^{-1} for CG and 13.83 h^{-1} for Amberlyst-15. However, CG displayed a higher selectivity toward the C15-18 compounds, indicating a greater intrinsic activity in consecutive aldol condensations. This leads to an increased production of heavy C15-18 adducts, which serve as valuable precursors for high-energy-density fuels.

On the other hand, the increased tendency to form trimers leads to a Carbon loss of approximately 14%, likely due to the formation of heavy compounds that are not detectable through GC/GC-MS analyses or deposited on the catalyst surface. This value well correlates with Y_{C15-18}, corresponding to 8% for the Amberlyst-15 sample and to zero for all the other catalysts. The molar distribution of the products as a function of the catalyst is depicted in Figure 7b. In accordance with the conversion values, when Y_{C15-18} is low, the cross-condensation of CHE is favored, and C11 concentration in the product mixture is 40%–46%, while C12 is around 30%. CPO self-condensation is remarkable only for the Amberlyst-15 sample (C_{C10} = 18%), together with

23667486, 2026, 5, Downloaded from https://advanced.onlinelibrary.wiley.com/doi/10.1002/adsu.70489 by Ilaria Braschi - Area Sistemi Dipart & Doc , Wiley Online Library on [11/05/2026]. See the Terms and Conditions (https://onlinelibrary.wiley.com/terms-and-conditions) on Wiley Online Library for rules of use; OA articles are governed by the applicable Creative Commons License

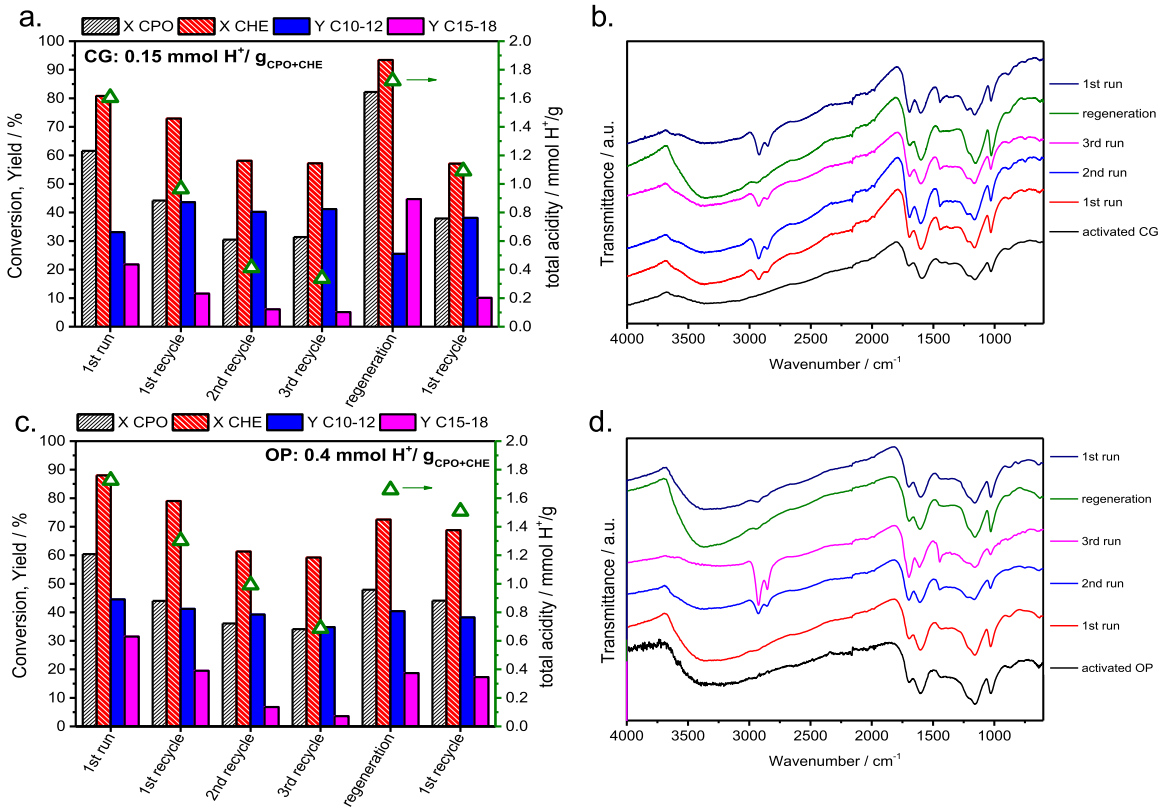

FIGURE 8 | Catalysts recyclability and regeneration in cross-aldol condensation expressed in terms of reagents conversion, products yield, and total acidity of the sample measured before each test: (a) activity and stability of sulfonated CG and (b) FT-ATR spectra of the sample before each test. Reaction conditions: CPO = 22 mmol, CHE = 22 mmol, T = 120°C, time = 4 h, catalyst amount = 0.15 mmol $H^+/g_{(CPO+CHE)}$. (c) catalytic activity and stability of activated OP, and (d) FT-ATR spectra of biochar before each test. Reaction conditions: CPO = 22 mmol, CHE = 22 mmol, T = 120°C, time = 4 h, catalyst amount = 0.40 mmol H^+ $g_{(CPO+CHE)}{}^{-1}$. CG: coffee grounds, OP: orange peel CPO: cyclopentanone, CHE: cyclohexanone.

cross-condensation products that hit a concentration of 40%. When trimers are formed, they are mainly composed of C17 compounds, likely originating from cross-condensation reaction between C6 and C11 molecules, while the formation of C16 boosts CPO conversion as in the case of the CG catalyst.

When tested over consecutive reaction cycles, the CG catalyst showed a gradual deactivation (Figure 8a), particularly in terms of CPO conversion (−28% after the first reaction cycle), which led to an increased yield of C10-12 compounds compared to the first cycle, but at the expense of a decreasing formation of trimers with consecutive recycles. Remarkably, similar C10-12 yields were obtained between the first and third reaction cycle with catalytic activity approaching a plateau after the two recycles. This loss of activity is attributable to a progressive reduction in catalyst acidity that, in accordance with the superior C15-18 yields, is likely related to the incremental deposition of heavy compounds on surface acid sites. This was confirmed by the FT-ATR spectra of the samples collected after each catalytic test. As shown in Figure 8b, the steady appearance of peaks attributable to the stretching vibrations of —CH_3 and —CH_2- (2850–2950 cm^{-1}) was observed, along with an increase in the relative intensity of the band around 1690 cm^{-1}, which is associated with conjugated C═O ketonic group vibrational modes. These functional groups are characteristics of the possible heavy reaction products, indicating their formation and gradual deposition on the catalyst surface during each reaction cycle. Interestingly, and somewhat unexpectedly, after the regeneration of the catalyst through a subsequent sulfonation (0.015 mL_{H2SO4} $mg_{BC}{}^{-1}$, 100°C for 1 h), CG exhibited a higher concentration of acid sites compared to the initial activation, reaching a value of 1.72 mmol H^+ g^{-1}. As a result, the catalytic activity increased, exceeding that recorded during the first cycle. The catalyst exhibited significantly higher CPO and CHE conversion values (82% and 93%, respectively) as well as the highest C15-18 yield under the tested conditions (45%). Although this particular behavior is difficult to fully rationalize, it is plausible that the progressive deposition of heavy compounds over successive reaction cycles increased the amount of organic material available for sulfonation during regeneration. On the other hand, the high activity results in a significant carbon loss (−16% during reaction) and a more pronounced deactivation in the subsequent cycle, where, despite retaining a good acidity concentration (1.09 mmol H^+ g^{-1}), the CG catalyst exhibits significantly lower performance.

In the case of the OP sample, performance comparable to that of the commercial resin was achieved by increasing the catalyst loading in the reaction, reaching a catalyst loading of 0.40 mmol H^+ $g_{(CPO+CHE)}{}^{-1}$. While minimizing catalyst usage remains a critical objective from an industrial perspective, it is important to highlight that the higher renewability and lower cost associated with BC-based catalysts may allow for greater flexibility in terms of their impact on the economic and environmental viability of the process. The catalytic activity obtained in these conditions is

23667486, 2026, 5, Downloaded from https://advanced.onlinelibrary.wiley.com/doi/10.1002/adsu.70489 by Ilaria Braschi - Area Sistemi Dipart & Doc , Wiley Online Library on [11/05/2026]. See the Terms and Conditions (https://onlinelibrary.wiley.com/terms-and-conditions) on Wiley Online Library for rules of use; OA articles are governed by the applicable Creative Commons License

reported in Figure 8c. Similarly to CG, the OP catalyst exhibited a higher tendency toward the production of C15-18 compounds ($Y_{C15\text{-}18}$ = 32%) compared to Amberlyst-15, while showing similar results in terms of reagent conversion. Also in this case, the catalyst exhibited a progressive deactivation over 4 reaction cycles corresponding to a steady (and almost linear) decrease in surface acidity after each catalytic run (from 1.73 to 0.69 mmol H^+ g_{cat}^{-1}). In this case, however, the catalyst showed a lower deactivation over consecutive reaction cycles compared to CG. This behavior is attributable to the combination of higher catalyst loading and lower intrinsic activity; the latter likely mitigated the deposition of heavy compounds onto the catalyst surface, as shown in Figure 8d. To rule out the possibility that the observed trend is due to the potential leaching of sulfonic groups under reaction conditions, a parallel test was performed on the OP catalyst. By maintaining a system acidity of 0.4 mmol H^+ $g_{(CPO+CHE)}^{-1}$, in this experiment, the catalyst was removed from the reaction mixture after 2 h, and then continuing the activity test without catalyst for a further 2 h. Throughout this period, the results reported in Figure S8 evidence that no variation in the reaction output was observed, excluding a significant occurrence of leaching phenomena during the aldol condensation process. Different from what was observed with CG, the subsequent sulfonation of the catalyst after four reaction cycles leads to a partial restoration of the acidic sites (96% of the initial, reaching a total acidity of 1.66 mmol H^+ g^{-1}). Although also in this case the regeneration was accompanied by the disappearance of the signal associated with the organic layer deposited during reactions (Figure 8d), the regenerated OP catalyst after four catalytic runs showed reduced catalytic activity compared to its initial performance, but displaying improved stability over an additional reaction cycle in terms of both reagents conversion and concentration of surface acidic sites (total acidity of 1.51 mmol H^+ g^{-1}).

To further investigate the involvement of the surface-active sites and monitor the reaction progress in real-time, in-situ FTIR experiments were performed using the OP catalyst. By comparing the spectra in Figure 9a (obtained by difference) and Figure S9, it was possible to observe the progressive depletion of the bends attributed to the C-H stretching of the two reactants, occurring concomitantly with the growth of two new bands at 2930 and 2857 cm^{-1} assigned to the formation of the condensation product. The latter bands shift toward lower wavenumbers as the reaction progresses, confirming the formation of trimeric species.

In the C═O stretching region (Figure 9b; Figure S9), a progressive erosion of the characteristic carbonyl bands of the reactants was observed, alongside the growth of a less intense band centered at 1720 cm^{-1}, ascribable to the C═O stretching mode of the condensation products. The appearance of a new band at 1620 cm^{-1}, attributable to the C═C stretching mode, strongly supports the analysis reported above. While identifying the preferential interaction with the catalytic active surface is complex, a comparison between the spectra of the fresh and spent (unwashed) catalyst (Figure 9d) reveals a band at 2968 cm^{-1} corresponding to the product adsorbed on the surface. Notably, the shifts observed for the bands at 1126 and 1159 cm^{-1} can be attributed to the interaction of the reactants with the sulfonic acid groups of the catalyst, confirming the direct involvement of the active sites in the catalytic process.

The OP catalyst was evaluated to assess the impact of increased reaction mass on the catalytic performance. The results obtained by scaling up the process by a factor of 3.5, reaching a total reactant mass of ~ 14 g (CPO = 77 mmol, CHE = 77 mmol, catalyst amount = 0.40 mmol H^+ $g_{(CPO+CHE)}^{-1}$) are reported in Figure S10a. Although a slight decrease in initial activity was observed compared to small-scale tests, the overall performance remained comparable, confirming the robustness of the OP catalyst. To further investigate catalyst stability under these conditions, multiple reaction-regeneration cycles were performed. As shown in Figure S10a, while a partial deactivation occurs after each run (in accordance with previous tests), the catalytic activity and total acidity were successfully restored after each regeneration step (labelled as a.r.). Notably, the catalyst was quantitatively recovered via filtration after each run. These findings demonstrate that the catalyst can be recycled multiple times without significantly affecting the final reaction output, proving its potential for sustainable long-term applications. To correlate this catalytic stability with the structural integrity of the material, XRD analysis was performed on both fresh sulfonated OP and spent catalyst collected after the final cycle (Figure S10b). Both patterns exhibit broad diffraction peaks characteristic of disordered amorphous carbon, centered at $2\theta \approx 20°$ and 40–50°, confirming that the core carbonaceous framework was preserved after prolonged exposure to reaction and regeneration conditions. Notably, the (002) reflection shifted from 22.67° in the fresh sample to 19.37° in the spent catalyst, corresponding to an increase in the interlaminar d_{002} spacing from 0.392 to 0.458 nm. This structural expansion is attributed to the inclusion of reaction intermediates or the rearrangement of functional groups between the sheets during the repeated cycles [25, 28]. Furthermore, a distinct pre-peak at 12.37° was observed, representing the expansion of specific domains due to the presence of bulky -SO_3H groups or hydrated species acting as spacers between the carbon layers. The persistence of these features confirms that the OP catalyst maintains its amorphous structure and, crucially, the accessibility of its active sites, supporting the robust catalytic performance observed over multiple runs.

2.4 | Green Metrics

To evaluate the environmental compatibility and sustainability of the proposed catalytic process, a comprehensive set of green metrics was calculated following the methodology reported in Table S2. The results of the cross-aldol condensation between CPO and CHE using sulfonated CG and OP under optimized conditions are reported in Table 3 (see Table S3 for a comparison with literature values). Atom Economy (AE) represents the theoretical yield for the reaction that was found to be 87.9%, indicating an intrinsically efficient pathway to produce SAF precursors where only water is generated as a byproduct. The Environmental Factor (E-factor) indicates the wastage of a process, the lower its value, the greater its sustainability. This value was as low as 0.59 for the OP catalyst, outperforming CG due to a better catalyst resistance toward fouling induced by heavy compound deposition. Directly related to these results, the Process Mass Intensity (PMI) and Mass Productivity (MP) correlate the total mass used in the process with the total amount of products formed (where a value of 1 or 100% indicates ideal

23667486, 2026, 5, Downloaded from https://advanced.onlinelibrary.wiley.com/doi/10.1002/adsu.70489 by ilaria braschi - Area Sistemi Dipart & Doc , Wiley Online Library on [11/05/2026]. See the Terms and Conditions (https://onlinelibrary.wiley.com/terms-and-conditions) on Wiley Online Library for rules of use; OA articles are governed by the applicable Creative Commons License

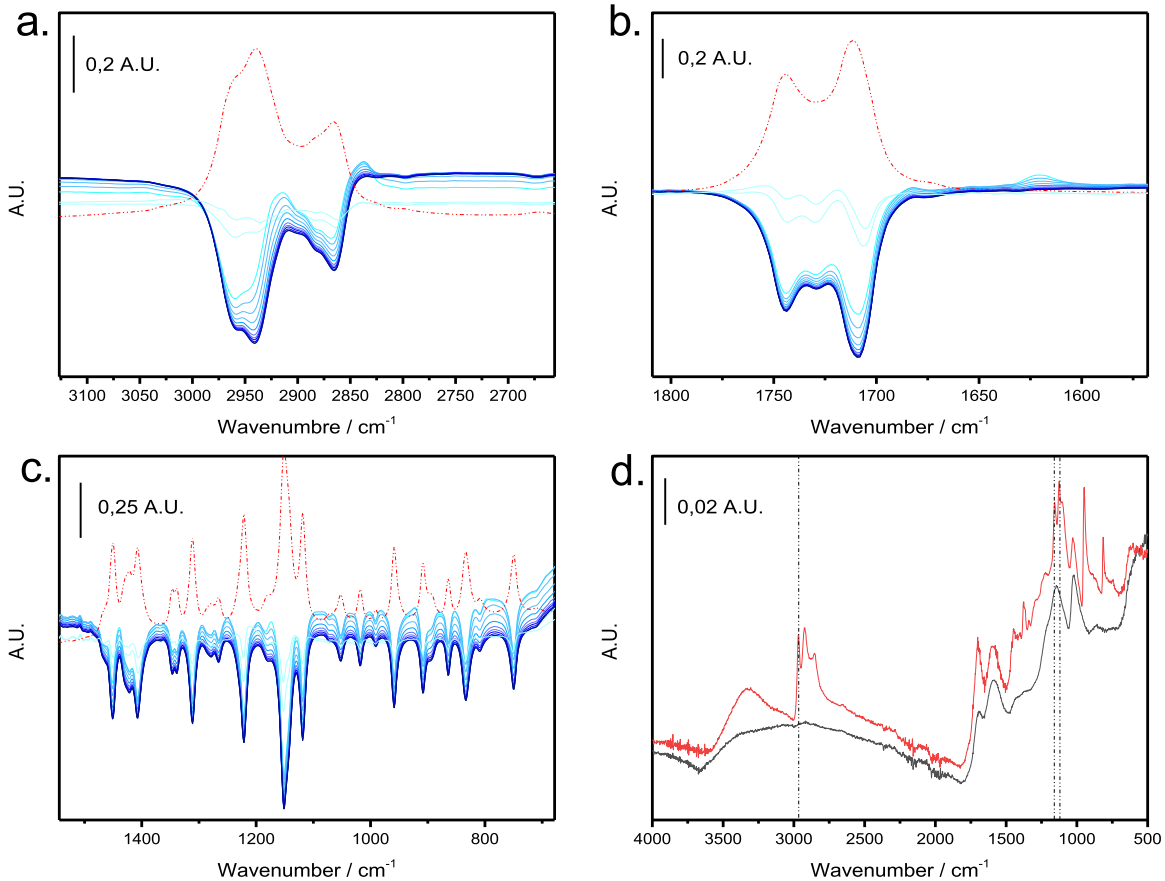

FIGURE 9 | In situ FT-ATR monitoring of the condensation reaction between CPO and CHE (1:1 mol/mol; catalyst loading 0.40 mmol H^+ $g_{(CPO+CHE)}^{-1}$). (a–c) show difference spectra obtained after subtraction of the initial reference spectrum (recorded at t = 0, T = 120°C); the color transition from light blue to dark indicates increasing reaction time. a) C-H stretching region; b) detail of the 1800–1600 cm^{-1} region; c) 1500–800 cm^{-1} region; d) FT-ATR spectra of the fresh OP catalyst (black line) and the spent (unwashed) catalyst after reaction (red line).

TABLE 3 | Green metric and intrinsic activity results for cross-aldol condensation between cyclopentanone and cyclohexanone over activated BC catalysts in optimized conditions (120°C, 4 h, 0.15 and 0.40 mmol H^+ $g_{(CPO+CHE)}^{-1}$ for CG and OP, respectively). CG: Coffee grounds, OP: Orange peel.

Parameter	CG	OP
Atom Economy [%]	87.92	87.92
Environmental Factor	0.95	0.59
Process Mass Intensity	1.95	1.59
Mass Productivity [%]	51.36	63.02
Carbon Economy [%]	58.09	71.25
Bio-based Carbon Index	1.00	1.00
Intrinsic Activity [$mol_{converted}$ $(mol\ H^+)^{-1}$ h^{-1}][a]	13.08	5.42

[a] calculated over 4 h of reaction

sustainability). Thanks to the solvent-free nature of the proposed reaction, PMI values of 1.59 and 1.94, and MP values 63% and 51% were calculated for OP and CG, respectively. In this case, the superior OP values are due to a higher reagent conversion and to a lower Carbon loss (C_{loss} of 9%) in optimized conditions. These results are further combined in the Carbon Economy metric, which highlights the enhanced (sustainability) performance of OP catalyst (71%) relative to CG (58%). It is noteworthy that these results do not directly match the calculated intrinsic activity of the samples (expressed as mol of converted reagents per mol of acid sites over 4 h for the first reaction cycle), where CG greatly surpassed OP. As previously noted, the greater tendency of CG to promote subsequent condensations, and thus the formation of C15-18 compounds, has a negative impact on catalyst fouling. This slightly decreases the overall efficiency of the batch process but likely makes this catalyst promising for use in continuous-flow processes, where the contact time between catalyst and reactants is limited.

23667486, 2026, 5, Downloaded from https://advanced.onlinelibrary.wiley.com/doi/10.1002/adsu.70489 by Ilaria braschi - Area Sistemi Dipart & Doc , Wiley Online Library on [11/05/2026]. See the Terms and Conditions (https://onlinelibrary.wiley.com/terms-and-conditions) on Wiley Online Library for rules of use; OA articles are governed by the applicable Creative Commons License

Finally, it is worth emphasizing that although commercial benchmarks like Amberlyst-15 would likely exhibit similar green metrics, given the comparable conversions and yields, the activated waste-derived BCs offer a distinct advantage in terms of the Bio-based Carbon Index (BCI). Indeed, our catalytic system operates with a BCI of 1.0, as both the reactants [57, 58] and catalyst support are derived from renewable biomass waste, unlike the petroleum-based matrix of commercial ion-exchange resins. This confirms that the use of waste-derived BCs not only ensures high catalytic efficiency but can also effectively close the loop of the circular economy in the production of SAF precursors.

3 | Conclusion

This study demonstrates the effective valorization of organic waste through low-temperature pyrolysis, producing bio-oil and BC with significant potential for various applications. The compositional analysis of bio-oils revealed a strong influence of the original feedstock on the distribution of chemical families, enabling the selective enrichment of valuable compounds such as furans, cyclic ketones, fatty acids, and aromatics. These results highlight promising routes for the downstream of bio-oils in green solvent production, renewable fuels, and chemical synthesis. The BCs obtained from the same feedstock exhibited distinct differences in carbonization degree and surface chemistry, suggesting multiple opportunities for their application in both environmental and technological fields. Upon sulfonation, BCs derived from OP and CG showed remarkable catalytic activity in reactions of industrial relevance, achieving high performance in the production of SAF precursors via cross-aldol condensation between CPO and CHE. The results were found to be competitive with those obtained using a commercial benchmark sulfonic resin, demonstrating how the high accessibility of acid sites on the surface of these low-specific-surface-area BCs can effectively promote the conversion of these bio-based ketones. Catalyst deactivation was observed to occur through a reversible fouling mechanism related to the formation and deposition of heavy compounds derived from C15-18 precursors, especially in the case of the highly active CG-based catalyst. Notably, these deposits could be effectively removed through a simple regeneration treatment, restoring catalytic active sites and performance.

4 | Experimental Section

4.1 | Biochar and Bio-Oil Production

The waste biomasses investigated were orange peel (OP), banana peel (BP), pineapple peel (PP), green waste (GW), and spent coffee grounds (CG). All peels were collected from the "Acquerello" nursery school located in Bologna (Italy). A few hours after collection, peels were placed into vessels and sun-dried for one week. To assure the complete drying, peels were put in the oven for 48 h at 60°C and then grinded and sieved at 0.5 mm. The final homogeneous powders were stored at 4°C before further experiments. Green waste was collected from a greengrocer putting together scraps of broad-leaved vegetables such as chard and lettuce. Scraps were dried at 60°C for 72 h, grinded and sieved at 0.5 mm, and finally, stored at 4°C. Spent coffee grounds were collected from domestic coffee brewing using a moka pot, dried at 60°C, and stored at 4°C.

Pyrolysis experiments were conducted using a stainless steel fixed-bed reactor placed into a tubular oven. After the pyrolysis section, the outlet stream passed through two condensers filled with acetone and maintained at −78°C for the collection of bio-oils. Biomass was dried at 110°C for 2 h and then placed into the isothermal zone of the reactor. In a typical experiment, N_2 is used as an inert gas and, after the total removal of air from the reaction environment, 2 g of biomass was heated up to 100°C and maintained at this temperature for 10 min. After equilibration, pyrolysis was carried out by increasing reactor temperature to 300°C–400°C for 1 h, using a constant heating rate of 10°C min^{-1} and a N_2 flow of 30 mL min^{-1}. After cooling, the collected bio-oil was concentrated and water removed using a rotavapor. The sample was then analyzed by the GC-MS technique using a Perkin Elmer Clarus 600 equipped with a DB-5 column. The amount of water and gas evolved during pyrolysis was determined by difference, based on the measured yields of BC and bio-oil.

4.2 | Biochar Activation Through Sulfonation

The different BCs were subjected to a sulfonation process using concentrated H_2SO_4. This treatment was carried out at atmospheric pressure in a 10 mL two-neck round flask reactor equipped with a reflux system and a thermometer. In a typical experiment, the H_2SO_4/BC dispersion was prepared using a ratio of 0.015 mL_{H2SO4} $mg_{BC}{}^{-1}$ and heated up to 100°C for 2 h under vigorous stirring. After cooling, the dispersion was diluted into 500 mL of deionized water, BC was recovered by filtration and washed several times with deionized water until neutral pH was reached. The BCs were dried in an oven maintained at 70°C for 24 h.

4.3 | Catalytic Activity

BCs were tested as heterogeneous catalysts for condensation and esterification reactions in solvent-free conditions. The catalytic tests were carried out at atmospheric pressure in a two-neck round flask reactor equipped with a condenser and a thermometer, placed into an oil bath used to heat up the system. For the aldol condensation reaction, 22 mmol of cyclopentanone (CPO), 22 mmol of cyclohexanone (CHE), and catalyst (0.15–0.40 mmol H^+ $g_{(CPO+CHE)}{}^{-1}$) were placed into the reaction system under stirring and heated up to 120°C for 4 h. For esterification reaction, 22 mmol of propionic acid (PA), 22 mmol of 1-butanol (BuOH) and catalyst (0.15 mmol H^+ $g_{(PA+BuOH)}{}^{-1}$) were placed into the reaction system under stirring and heated up to 80°C for 4 h. After reaction, the system was quenched in an ice-bath and the reaction mixture quantitatively analyzed using decane as internal standard in a GC Autosystem XL (Perkin Elmer) equipped with a DB-5 column and an FID detector. Amberlyst-15 (4.70 mmol H^+/g) benchmark catalyst was purchased from Sigma–Aldrich. The catalytic activity of the sample was evaluated using the following equations.

23667486, 2026, 5, Downloaded from https://advanced.onlinelibrary.wiley.com/doi/10.1002/adsu.70489 by Ilaria braschi - Area Sistemi Dipart & Doc , Wiley Online Library on [11/05/2026]. See the Terms and Conditions (https://onlinelibrary.wiley.com/terms-and-conditions) on Wiley Online Library for rules of use; OA articles are governed by the applicable Creative Commons License

Conversion

$$X_{(\mathrm{CPO,\ CHE})} = \frac{(mol\ CPO,\ CHE\ t_0 - mol\ CPO, CHE)}{mol\ CPO, CHE\ t_0} \times 100$$

Yield

$$Y_{C10-12} = \frac{2\ mol\ C_{10-12}}{mol\ CPO + CHE\ t_0} \times 100;$$

$$Y_{C15-18} = \frac{3\ mol\ C_{15-18}}{mol\ CPO + CHE\ t_0} \times 100$$

$$\mathrm{C\ loss} = \frac{[\mathrm{mol\ CPO\ t_0} + \mathrm{\ mol\ CHE\ t_0} - (\mathrm{mol\ CPO} + \mathrm{\ mol\ CHE} + 2\ \mathrm{mol\ C_{10-12}} + 3\ \mathrm{mol\ C_{15-18}})]}{mol\ CPO\ t_0 + mol\ CHE\ t_0} \times 100$$

4.4 | Characterization of Materials

The IR spectra of the materials were acquired in attenuated total reflectance (ATR) over the 600–4000 cm^{-1} range using a Thermo Scientific Nicolet iS10 Smart iTR equipped with a Smart OMNI transmission instrument. The samples morphology was investigated through SEM observation using a FEI/Phillips XL30 ESEM instrument. The semi-quantitative elemental analysis was carried out with an x-ray energy dispersive spectrometer, EDAX AMETEK Element, coupled with SEM. The EDX detector was a silicon drift detector with a silicon nitride window. Porosity data and surface areas were determined by N_2 adsorption/desorption at -196°C using a Micromeritics ASAP 2020 instrument. In a typical experiment, 0.150 g of the sample was pretreated under vacuum at 150°C for 1 h, pore size distribution was calculated through the Barret-Joyner-Halenda (BJH) analysis method, and the specific surface area through the Brunauer-Emmet-Teller (BET) multiple-point method. The concentration of acid/basic sites per gram of material was determined by a titration with an aqueous solution of NaOH or HCl (5 mM). In a typical titration, 50 mg of material was dispersed in 50 mL of deionized water under vigorous stirring. After stabilization and measurement of the initial pH (using a pH meter), the NaOH or HCl solution was added dropwise until the initial pH was reached [54]. BC proximate analyses were conducted through TG-DSC experiments by means of a Netzsch STA 409 PC instrument. Samples were placed in alumina crucibles and maintained at 110°C for 2 h under a pure N_2 atmosphere. After that, the samples were heated up to 900°C (10°C min^{-1}) and maintained at this temperature for 2 h. Volatiles content was calculated considering the percentage of mass lost during the experiment after moisture removal. Fixed carbon value corresponds to the percentage of mass that is not degraded during TG analysis minus the ash content determined by performing the same TG analysis under synthetic air instead of N_2. CHN analyses were performed using a Perkin Elmer CHN analyzer 2400 Series II, with O concentration determined by difference. Starting from these data, higher heating value (HHV) of biochar samples was also determined by using the formula: HHV = (33.5 C + 142.3 H − 15.4 O − 14.5 N) / 100 [59]. The contact angle measurements were carried out using an Ossila Contact Angle Goniometer L2004A. Biochar was pressed (10 tons) into a tablet and dried at 110°C for 2 h before the deposition of three droplets (2 μL each) on its surface. The contact angle values were determined considering both the visible angles per each droplet, so as to calculate an average value based on six measurements. Mechanistic investigation has been carried out via in situ FT-ATR experiments using a Bruker Tensor II instrument equipped with an ATR cell configured with a sealed gasket and glass on top, enabling the reaction to be performed at 120°C. The spectra reported in the text are obtained by subtracting each spectrum to the first spectrum acquired at room temperature. Powder XRD analyses were performed on a Rigaku Miniflex 600 diffractometer equipped with a copper anode. Samples were recorded in a 2θ range of 5°-80° with a step size of 0.05° and a scan step time of 12.25 s.

Acknowledgements

Scientific support from the CRIETT centre of the University of Insubria (instrument codes: MAC02, MAC04, MAC08, MAC09) is greatly acknowledged.

Open access publishing facilitated by Universita degli Studi dell'Insubria, as part of the Wiley - CRUI-CARE agreement.

Conflicts of Interest

The authors declare no conflicts of interest.

Data Availability Statement

The data that support the findings of this study are available in the supplementary material of this article.

References

1. N. Schiaroli, M. Battisti, P. Benito, et al., "Catalytic Upgrading of Clean Biogas to Synthesis Gas," *Catalysts* 12 (2022): 109, https://doi.org/10.3390/catal12020109.

2. N. Schiaroli, C. Lucarelli, M. C. Iapalucci, G. Fornasari, A. Crimaldi, and A. Vaccari, "Combined Reforming of Clean Biogas Over Nanosized Ni–Rh Bimetallic Clusters," *Catalysts* 10 (2020): 1345, https://doi.org/10.3390/catal10111345.

3. N. Schiaroli, L. Negahdar, M. Lützen, et al., "Efficient Low-Loaded Ternary Pd-In_2O_3-Al_2O_3 Catalysts for Methanol Production," *Journal of Catalysis* 424 (2023): 140–151, https://doi.org/10.1016/j.jcat.2023.05.012.

4. M. E. Potter, S. Mediavilla Madrigal, E. Campbell, et al., "A High Pressure Operando Spectroscopy Examination of Bimetal Interactions in 'Metal Efficient' Palladium/In 2 O 3 /Al_2O_3 Catalysts for CO_2 Hydrogenation," *Angewandte Chemie International Edition* 62 (2023): 202312645, https://doi.org/10.1002/anie.202312645.

5. N. Schiaroli, L. Scaglione, R. Mandioni, F. Foschi, S. Recchia, and C. Lucarelli, "Cu-Based Catalysts for the One-Pot Condensation–Hydrogenation of Cyclopentanone to Produce Valuable SAF Precursors," *Chemcatchem* 17 (2025): 202401586, https://doi.org/10.1002/cctc.202401586.

23667486, 2026, 5, Downloaded from https://advanced.onlinelibrary.wiley.com/doi/10.1002/adsu.70489 by ilaria braschi - Area Sistemi Dipart & Doc , Wiley Online Library on [11/05/2026]. See the Terms and Conditions (https://onlinelibrary.wiley.com/terms-and-conditions) on Wiley Online Library for rules of use; OA articles are governed by the applicable Creative Commons License

6. L. Grazia, T. Della Rosa, D. Bonincontro, et al., "CaO as a Cheap, Eco-Friendly Material for the Continuous-Flow, Gas-Phase, Catalytic Transfer Hydrogenation of Furfural With Methanol," *Catalysis Today* 420 (2023): 114036, https://doi.org/10.1016/j.cattod.2023.02.01.

7. J. De Maron, L. Bellotti, A. Baldelli, et al., "Evaluation of the Catalytic Activity of Metal Phosphates and Related Oxides in the Ketonization of Propionic Acid," *Sustainable Chemistry* 3 (2022): 58–75, https://doi.org/10.3390/suschem3010005.

8. R. C. Saxena, D. Seal, S. Kumar, and H. B. Goyal, "Thermo-Chemical Routes for Hydrogen Rich Gas From Biomass: a Review," *Renewable and Sustainable Energy Reviews* 12 (2008): 1909–1927, https://doi.org/10.1016/j.rser.2007.03.005.

9. Y. Li, R. Gupta, Q. Zhang, and S. You, "Review of Biochar Production via Crop Residue Pyrolysis: Development and Perspectives," *Bioresource Technology* 369 (2023): 128423, https://doi.org/10.1016/j.biortech.2022.128423.

10. A. Selvarajoo, Y. L. Wong, K. S. Khoo, W. H. Chen, and P. L. Show, "Biochar Production via Pyrolysis of Citrus Peel Fruit Waste as a Potential Usage as Solid Biofuel," *Chemosphere* 294 (2022): 133671, https://doi.org/10.1016/j.chemosphere.2022.133671.

11. A. Ibn Ferjani, M. Jeguirim, S. Jellali, et al., "The Use of Exhausted Grape Marc to Produce Biofuels and Biofertilizers: Effect of Pyrolysis Temperatures on Biochars Properties," *Renewable and Sustainable Energy Reviews* 107 (2019): 425–433, https://doi.org/10.1016/j.rser.2019.03.034.

12. S. S. Lam, R. K. Liew, C. K. Cheng, et al., "Pyrolysis Production of Fruit Peel Biochar for Potential Use in Treatment of Palm Oil Mill Effluent," *Journal of Environmental Management* 213 (2018): 400–408, https://doi.org/10.1016/j.jenvman.2018.02.092.

13. S. Ao, P. Dwivedi, A. P. Chowdhury, S. Lallianrawna, A. Dhakshinamoorthy, and S. L. Rokhum, "Paper Waste-derived Functionalized Biochar Catalyst for Production of Biodiesel Using Jatropha Curcas Oil Feedstock," *Bioresource Technology Reports* 29 (2025): 102031, https://doi.org/10.1016/j.biteb.2025.102031.

14. Z. Wu, Y. Deng, F. Tian, et al., "N-doped Biochar Supported Ni-Co Alloy Catalyst for Efficient Hydrocracking of Enzymatic Hydrolysis Lignin to Monophenols in Water," *Chemical Engineering Journal* 505 (2025): 159424, https://doi.org/10.1016/j.cej.2025.159424.

15. Y. Yuan, L. Huang, M. Yilmaz, T. C. Zhang, Y. Wang, and S. Yuan, "$MgFe_2O_4$-Loaded N-Doped Biochar derived From Waste Cooked Rice for Efficient Low-Temperature Desulfurization of H_2S," *Fuel* 339 (2023): 127385, https://doi.org/10.1016/j.fuel.2022.127385.

16. Y. Li and P. T. Williams, "Catalytic Conversion of Biomass Components and Waste Biomass for Hydrogen/Syngas Production Using Biochar Catalysts," *Biomass and Bioenergy* 194 (2025): 107675, https://doi.org/10.1016/j.biombioe.2025.107675.

17. S. Z. Zhang, Z. S. Cui, M. Zhang, and Z. H. Zhang, "Biochar-based Functional Materials as Heterogeneous Catalysts for Organic Reactions," *Current Opinion in Green and Sustainable Chemistry* 38 (2022): 100713, https://doi.org/10.1016/j.cogsc.2022.100713.

18. L. N. Dong, Y. M. Wang, W. L. Zhang, L. P. Mo, and Z. H. Zhang, "Nickel Supported on Magnetic Biochar as a Highly Efficient and Recyclable Heterogeneous Catalyst for the One-Pot Synthesis of Spirooxindole-Dihydropyridines," *Applied Organometallic Chemistry* 36 (2022): 6667, https://doi.org/10.1002/aoc.6667.

19. H. Wang, C. Qiao, C. Chen, et al., "Synergistic Adsorption and Singlet Oxygenation of Humic Acid on Alkali-activated Biochar via Peroxymonosulfate Activation," *Chinese Chemical Letters* 36 (2025): 110244, https://doi.org/10.1016/j.cclet.2024.110244.

20. Q. Xie, X. Yang, K. Xu, Z. Chen, B. Sarkar, and X. Dou, "Conversion of Biochar to Sulfonated Solid Acid Catalysts for Spiramycin Hydrolysis: Insights Into the Sulfonation Process," *Environmental Research* 188 (2020): 109887, https://doi.org/10.1016/j.envres.2020.109887.

21. X. Dong, Y. Chu, Z. Tong, et al., "Mechanisms of Adsorption and Functionalization of Biochar for Pesticides: a Review," *Ecotoxicology and Environmental Safety* 272 (2024): 116019, https://doi.org/10.1016/j.ecoenv.2024.116019.

22. M. Saidi, M. Safaripour, F. A. Ameri, and M. E. Jomeh, "Application of Sulfonated Biochar-based Magnetic Catalyst for Biodiesel Production: Sensitivity Analysis and Process Optimization," *Chemical Engineering and Processing – Process Intensification* 190 (2023): 109419, https://doi.org/10.1016/j.cep.2023.109419.

23. N. Kumari, T. Chhabra, S. Kumar, and V. Krishnan, "Nanoarchitectonics of Sulfonated Biochar From Pine Needles as Catalyst for Conversion of Biomass Derived Chemicals to Value Added Products," *Catalysis Communications* 168 (2022): 106467, https://doi.org/10.1016/j.catcom.2022.106467.

24. X. Xiong, I. K. M. Yu, S. S. Chen, et al., "Sulfonated Biochar as Acid Catalyst for Sugar Hydrolysis and Dehydration," *Catalysis Today* 314 (2018): 52–61, https://doi.org/10.1016/j.cattod.2018.02.034.

25. T. Chhabra, P. Dwivedi, and V. Krishnan, "Acid Functionalized Hydrochar as Heterogeneous Catalysts for Solventless Synthesis of Biofuel Precursors," *Green Chemistry* 24 (2022): 898–910, https://doi.org/10.1039/D1GC03330A.

26. Y. Zhong, Q. Deng, Q. Yao, et al., "Functionalized Biochar With Superacidity and Hydrophobicity as a Highly Efficient Catalyst in the Synthesis of Renewable High-density Fuels," *ACS Sustainable Chemistry & Engineering* 8 (2020): 7785–7794, https://doi.org/10.1021/acssuschemeng.9b07367.

27. D. Chen, K. Cen, X. Zhuang, et al., "Insight Into Biomass Pyrolysis Mechanism Based on Cellulose, Hemicellulose, and Lignin: Evolution of Volatiles and Kinetics, Elucidation of Reaction Pathways, and Characterization of Gas, Biochar and Bio-Oil," *Combustion and Flame* 242 (2022): 112142, https://doi.org/10.1016/j.combustflame.2022.112142.

28. M. Keiluweit, P. S. Nico, M. G. Johnson, and M. Kleber, "Dynamic Molecular Structure of Plant Biomass-derived Black Carbon (Biochar)," *Environmental Science & Technology* 44 (2010): 1247–1253, https://doi.org/10.1021/es9031419.

29. C. Y. Jeong, S. K. Dodla, and J. J. Wang, "Fundamental and Molecular Composition Characteristics of Biochars Produced From Sugarcane and Rice Crop Residues and by-products," *Chemosphere* 142 (2016): 4–13, https://doi.org/10.1016/j.chemosphere.2015.05.084.

30. A. Raheem, L. Ding, Q. He, et al., "Effective Pretreatment of Corn Straw Biomass Using Hydrothermal Carbonization for Co-Gasification With Coal: Response Surface Methodology–Box Behnken Design," *Fuel* 324 (2022): 124544, https://doi.org/10.1016/j.fuel.2022.124544.

31. B. Ameha, T. T. Nadew, T. S. Tedla, B. Getye, D. A. Mengie, and S. Ayalneh, "The Use of Banana Peel as a Low-Cost Adsorption Material for Removing Hexavalent Chromium From Tannery Wastewater: Optimization, Kinetic and Isotherm Study, and Regeneration Aspects," *RSC Advances* 14 (2024): 3675–3690, https://doi.org/10.1039/D3RA07476E.

32. E. Arriola-Villaseñor, A. N. Ardila A, Z. R. Barrera, and J. Hernández, "Using Banana Waste Biochar for Simultaneous Removal of Heavy Metals From Raw Real Wastewater From the Electroplating Industry," *Desalination and Water Treatment* 314 (2023): 88–102, https://doi.org/10.5004/dwt.2023.30079.

33. S. Xue, X. Zhang, H. H. Ngo, et al., "Food Waste Based Biochars for Ammonia Nitrogen Removal From Aqueous Solutions," *Bioresource Technology* 292 (2019): 121927, https://doi.org/10.1016/j.biortech.2019.121927.

34. R. Mallampati, L. Xuanjun, A. Adin, and S. Valiyaveettil, "Fruit Peels as Efficient Renewable Adsorbents for Removal of Dissolved Heavy Metals and Dyes From Water," *ACS Sustainable Chemistry & Engineering* 3 (2015): 1117–1124, https://doi.org/10.1021/acssuschemeng.5b00207.

35. P. Gosalvitr, R. M. Cuéllar-Franca, R. Smith, and A. Azapagic, "Environmental and Economic Sustainability Assessment of the Production and Consumption of Different Types of Coffee in the UK," *Sustainable Production and Consumption* 49 (2024): 144–162, https://doi.org/10.1016/j.spc.2024.06.004.

23667486, 2026, 5, Downloaded from https://advanced.onlinelibrary.wiley.com/doi/10.1002/adsu.70489 by Ibrà braschi - Area Sistemi Dipart & Doc , Wiley Online Library on [11/05/2026]. See the Terms and Conditions (https://onlinelibrary.wiley.com/terms-and-conditions) on Wiley Online Library for rules of use; OA articles are governed by the applicable Creative Commons License

36. S. Nanda, P. Mohanty, K. K. Pant, S. Naik, J. A. Kozinski, and A. K. Dalai, "Characterization of North American Lignocellulosic Biomass and Biochars in Terms of Their Candidacy for Alternate Renewable Fuels," *BioEnergy Research* 6 (2012): 663–677, https://doi.org/10.1007/s12155-012-9281-4.

37. M. Puccini, D. Licursi, E. Stefanelli, S. Vitolo, A. M. Raspolli Galletti, and H. J. Heeres, "Levulinic Acid From Orange Peel Waste by Hydrothermal Carbonization (HTC)," *Chemical Engineering Transactions* 50 (2016): 223–228, https://doi.org/10.3303/CET1650038.

38. C. M. Chandrasekar, H. Krishnamachari, S. Farris, and D. Romano, "Development and Characterization of Starch-based Bioactive Thermoplastic Packaging Films Derived From Banana Peels," *Carbohydrate Polymer Technologies and Applications* 5 (2023): 100328, https://doi.org/10.1016/j.carpta.2023.100328.

39. T. Jóźwiak, U. Filipkowska, J. Struk-Sokolowska, et al., "The Use of Spent Coffee Grounds and Spent Green Tea Leaves for the Removal of Cationic Dyes From Aqueous Solutions," *Scientific Reports* 11 (2021): 9584, https://doi.org/10.1038/s41598-021-89095-6.

40. B. Arwenyo, J. J. Varco, A. Dygert, S. Brown, C. U. Pittman, and T. Mlsna, "Contribution of Modified P-enriched Biochar on pH Buffering Capacity of Acidic Soil," *Journal of Environmental Management* 339 (2023): 117863, https://doi.org/10.1016/j.jenvman.2023.117863.

41. S. Zhang, Q. Zhu, W. de Vries, et al., "Effects of Soil Amendments on Soil Acidity and Crop Yields in Acidic Soils: a World-wide Meta-analysis," *Journal of Environmental Management* 345 (2023): 118531, https://doi.org/10.1016/j.jenvman.2023.118531.

42. S. Adhikari, M. A. Parvez Mahmud, M. D. Nguyen, and W. Timms, "Evaluating Fundamental Biochar Properties in Relation to Water Holding Capacity," *Chemosphere* 328 (2023): 138620, https://doi.org/10.1016/j.chemosphere.2023.138620.

43. W. Kang and Z. Zhang, "Selective Production of Acetic Acid via Catalytic Fast Pyrolysis of Hexoses Over Potassium Salts," *Catalysts* 10 (2020): 502, https://doi.org/10.3390/catal10050502.

44. Y. Zhao, K. Lu, H. Xu, L. Zhu, and S. Wang, "A Critical Review of Recent Advances in the Production of Furfural and 5-Hydroxymethylfurfural From Lignocellulosic Biomass Through Homogeneous Catalytic Hydrothermal Conversion," *Renewable and Sustainable Energy Reviews* 139 (2021): 110706, https://doi.org/10.1016/j.rser.2021.110706.

45. D. Bonincontro, A. Lolli, A. Storione, et al., "Pt and Pt/Sn Carbonyl Clusters as Precursors for the Synthesis of Supported Metal Catalysts for the Base-free Oxidation of HMF," *Applied Catalysis A: General* 588 (2019): 117279, https://doi.org/10.1016/j.apcata.2019.117279.

46. A. Hart, J. A. Onwudili, E. Yildirir, and S. E. Hashmnezhad, "Energy-dense Sustainable Aviation Fuel-range Hydrocarbons From Cyclohexanone as a Biomass-derived Feedstock via Sequential Catalytic Aldol Condensation and Hydrodeoxygenation," *Chemical Engineering Journal* 509 (2025): 161494, https://doi.org/10.1016/j.cej.2025.161494.

47. N. Schiaroli, F. Foschi, M. Mella, and C. Lucarelli, "C-Acylation of Guaiacol With Acetic Acid Over Solid Acid Catalysts Under Mild Reaction Conditions," *Chemcatchem* 17 (2025): 01112, https://doi.org/10.1002/cctc.202501112.

48. X. Lv, C. Zhao, N. Yan, X. Ma, S. Feng, and L. Shuai, "Sustainable Aviation Fuel (SAF) From lignin: Pathways, Catalysts, and Challenges," *Bioresource Technology* 419 (2025): 132039, https://doi.org/10.1016/j.biortech.2025.132039.

49. D. Munick de Albuquerque Fragoso, F. P. Bouxin, J. R. D. Montgomery, N. J. Westwood, and S. D. Jackson, "Catalytic Depolymerisation of Isolated Lignin to Fine Chemicals: Depolymerisation of Kraft Lignin," *Bioresource Technology Reports* 9 (2020): 100400, https://doi.org/10.1016/j.biteb.2020.100400.

50. M. A. Peters, C. T. Alves, J. Wang, and J. A. Onwudili, "Subcritical Water Hydrolysis of Fresh and Waste Cooking Oils to Fatty Acids Followed by Esterification to Fatty Acid Methyl Esters: Detailed Characterization of Feedstocks and Products," *ACS Omega* 7 (2022): 46870–46883, https://doi.org/10.1021/acsomega.2c05972.

51. I. Johansson and M. Svensson, "Surfactants Based on Fatty Acids and Other Natural Hydrophobes," *Current Opinion in Colloid & Interface Science* 6 (2001): 178–188, https://doi.org/10.1016/S1359-0294(01)00076-0.

52. E. Hu, K. Xu, D. Xu, D. Liu, and L. Zhao, "Facile Preparation of Sulfonated Biochar Derived From Spent Coffee Grounds for Efficient Hydrogen Production From Methanolysis of Sodium Borohydride," *International Journal of Hydrogen Energy* 116 (2025): 211–220, https://doi.org/10.1016/j.ijhydene.2025.03.108.

53. K. Ngaosuwan, J. G. Goodwin Jr., and P. Prasertdham, "A Green Sulfonated Carbon-Based Catalyst Derived From Coffee Residue for Esterification," *Renewable Energy* 86 (2016): 262–269, https://doi.org/10.1016/j.renene.2015.08.010.

54. N. Schiaroli, A. Allegri, M. Eberle, et al., "Superacid Resin-Based Heterogeneous Catalysts for the Selective Acylation of 1,2-Methylenedioxybenzene," *Chemsuschem* 16 (2023): 202300903, https://doi.org/10.1002/cssc.202300903.

55. P. Benito, A. Vaccari, C. Antonetti, et al., "Tunable Copper-Hydrotalcite Derived Mixed Oxides for Sustainable Ethanol Condensation to n-Butanol in Liquid Phase," *Journal of Cleaner Production* 209 (2019): 1614–1623, https://doi.org/10.1016/j.jclepro.2018.11.150.

56. K. V. Bhavsar and G. D. Yadav, "Microwave Assisted Solvent-free Synthesis of n-butyl Propionate by Immobilized Lipase as Catalyst," *Biocatalysis and Agricultural Biotechnology* 14 (2018): 264–269, https://doi.org/10.1016/j.bcab.2018.02.012.

57. J. Zhang, X. Kuang, L. Zhu, X. Xiao, Z. Zhou, and F. Qi, "Sustainable Production of Cyclohexanones Through Hydrodeoxygenation of Lignin-Derived Phenolics Over PdFe/HZSM-5 Catalysts," *Fuel* 383 (2025): 133863, https://doi.org/10.1016/j.fuel.2024.133863.

58. A. Patil, M. Engelbert van Bevervoorde, and F. Neira d'Angelo, "Intensifying Cyclopentanone Synthesis From furfural Using Supported Copper Catalysts," *Chemsuschem* 18 (2025): 202401484, https://doi.org/10.1002/cssc.202401484.

59. S. G. Sahu, P. Sarkar, N. Chakraborty, and A. K. Adak, "Thermogravimetric Assessment of Combustion Characteristics of Blends of a Coal With Different Biomass Chars," *Fuel Processing Technology* 91 (2010): 369–378, https://doi.org/10.1016/j.fuproc.2009.12.0012.

Supporting Information

Additional supporting information can be found online in the Supporting Information section.

Supporting File: adsu70489-sup-0001-SuppMat.pdf.

23667486, 2026, 5, Downloaded from https://advanced.onlinelibrary.wiley.com/doi/10.1002/adsu.70489 by ibria braschi - Area Sistemi Dipart & Doc , Wiley Online Library on [11/05/2026]. See the Terms and Conditions (https://onlinelibrary.wiley.com/terms-and-conditions) on Wiley Online Library for rules of use; OA articles are governed by the applicable Creative Commons License